Ca2+ Puffs Originate from Preestablished Stable Clusters of Inositol Trisphosphate Receptors

Ian F. Smith, Steven M. Wiltgen, Jianwei Shuai and Ian Parker (24 November 2009)

Science Signaling **2** (98), ra77. [DOI: 10.1126/scisignal.2000466]

CALCIUM SIGNALING

Ca^{2+} Puffs Originate from Preestablished Stable Clusters of Inositol Trisphosphate Receptors

Ian F. Smith,[1]* Steven M. Wiltgen,[1] Jianwei Shuai,[2] Ian Parker[1,3]

(Published 24 November 2009; Volume 2 Issue 98 ra77)

Intracellular calcium ion (Ca^{2+}) signaling crucially depends on the clustered organization of inositol trisphosphate receptors (IP_3Rs) in the endoplasmic reticulum (ER) membrane. These ligand-gated ion channels liberate Ca^{2+} to generate local signals known as Ca^{2+} puffs. We tested the hypothesis that IP_3 itself elicits rapid clustering of IP_3Rs by using flash photolysis of caged IP_3 in conjunction with high-resolution Ca^{2+} imaging to monitor the activity and localization of individual IP_3Rs within intact mammalian cells. Our results indicate that Ca^{2+} puffs arising with latencies as short as 100 to 200 ms after photorelease of IP_3 already involve at least four IP_3R channels, and that this number does not subsequently grow. Moreover, single active IP_3Rs show limited mobility, and stochastic simulations suggest that aggregation of IP_3Rs at puff sites by a diffusional trapping mechanism would require many seconds. We thus conclude that puff sites represent preestablished, stable clusters of IP_3Rs and that functional IP_3Rs are not readily diffusible within the ER membrane.

INTRODUCTION

Inositol trisphosphate receptors (IP_3Rs) are Ca^{2+}-permeable channels in the membrane of the endoplasmic reticulum (ER) that liberate Ca^{2+} sequestered in ER stores to generate cytosolic Ca^{2+} signals that control diverse cellular functions including secretion, synaptic plasticity, and gene expression (*1*). Opening of the IP_3R channel is regulated by the soluble second messenger IP_3, which is produced in response to activation of numerous heterotrimeric guanine nucleotide–binding protein (G protein)– and tyrosine kinase–linked cell surface receptors (*2*). However, IP_3R channel gating also requires cytosolic Ca^{2+} itself (*2*, *3*), creating a positive feedback mechanism of Ca^{2+}-induced Ca^{2+} release (CICR), whereby release of Ca^{2+} through one IP_3R channel will tend to promote the opening of neighboring channels. To appropriately control this potentially explosive regenerative process, IP_3Rs are distributed in clusters across the ER surface (*2*). This results in a hierarchical organization of Ca^{2+} signals involving stochastic recruitment of varying numbers of IP_3Rs (*4*–*6*). Ca^{2+} release may be restricted to only a single channel, resulting in a tiny Ca^{2+} signal known as a blip, or opening of one channel may trigger other IP_3Rs within a cluster to generate a larger local Ca^{2+} signal known as a puff. Finally, higher concentrations of IP_3 may evoke Ca^{2+} waves that propagate throughout the cell in a saltatory manner through recruitment of multiple puff sites by successive cycles of Ca^{2+} diffusion and CICR. The spatial localization of IP_3Rs is thus crucial for establishing and optimizing the spatiotemporal patterning of cytosolic Ca^{2+} signals that ensures appropriate regulation of downstream signaling pathways (*7*). However, important questions remain regarding how IP_3Rs aggregate into clusters and how this clustered organization is maintained.

Fluorescence Ca^{2+} imaging studies in *Xenopus* oocytes and various mammalian cell lines indicate that numerous puffs arise over many minutes at fixed locations within the cell, suggesting that IP_3R clusters are relatively stable (*8*–*11*). However, imaging studies with green fluorescent protein (GFP)–tagged or immunostained IP_3Rs indicate that IP_3Rs can diffuse within the ER membrane (*12*–*20*), and that in resting cells they display a reticular pattern resembling that of other ER-localized proteins (*11*–*14*, *16*–*21*), suggesting that they are freely distributed throughout the ER. Several publications describe the aggregation of IP_3Rs into clusters after sustained activation of IP_3 signaling or cytosolic [Ca^{2+}] elevation or both (*12*, *17*–*20*). In particular, recent studies (*22*, *23*) using patch-clamp recordings of excised nuclei from DT40 cells stably expressing type 1 or type 3 IP_3Rs showed that IP_3Rs are freely diffusible within the lipid membrane and that they rapidly (within a few seconds) cluster together when [IP_3] rises, resulting in a reduction of mean channel open probability and open duration through postulated protein-protein interactions. Based on these findings, the authors hypothesized that IP_3 may regulate the assembly and behavior of Ca^{2+} puff sites under physiological conditions (*22*).

Here, we tested this hypothesis of rapid and dynamic IP_3R clustering by using total internal reflection fluorescence (TIRF) microscopy to resolve Ca^{2+} transients arising from openings of individual IP_3R channels in intact mammalian cells (*24*). We found that puffs arising 100 to 200 ms after photorelease of IP_3 involved no fewer IP_3R channels than did puffs occurring several seconds later. Moreover, sites at which only a single IP_3R was active remained at fixed locations. We thus conclude that puff sites represent preestablished, stable clusters of IP_3Rs and that functional IP_3Rs are not readily diffusible within the ER membrane.

RESULTS

Puff and blip sites imaged with TIRF microscopy

We began by determining the numbers of IP_3R channels contributing to puffs evoked at different times after a step increase in [IP_3]. We loaded SH-SY5Y neuroblastoma cells with the fluorescent Ca^{2+} indicator fluo-4, together with a photolabile caged precursor [ci-IP_3 (D-2,3-*O*-isopropylidene-6-*O*-(2-nitro-4,5-dimethoxy)benzyl-*myo*-inositol 1,4,5-trisphosphate)] of the slowly-metabolized IP_3 analog i-IP_3 and with the Ca^{2+} buffer EGTA, by incubating them with membrane-permeant esters of these compounds. We then used TIRF microscopy to image local Ca^{2+} events evoked by delivering brief flashes of ultraviolet (UV) light to photorelease i-IP_3. Fluo-4 fluorescence signals closely reflect instantaneous Ca^{2+} flux from the ER under these conditions because of the extremely thin (~100 nm) optical

[1]Department of Neurobiology and Behavior, University of California, Irvine, CA 92697–4550, USA. [2]Department of Physics, Xiamen University, Xiamen 361005, China. [3]Department of Physiology and Biophysics, University of California, Irvine, CA 92697–4550, USA.
*To whom correspondence should be addressed. E-mail: ismith@uci.edu

section of TIRF microscopy in conjunction with the use of the slow Ca^{2+} buffer EGTA to suppress Ca^{2+} waves and "sharpen" local Ca^{2+} gradients (*25*), making it possible to resolve Ca^{2+} flux through single IP_3Rs (*9*).

Cells were essentially quiescent with regard to Ca^{2+} signals before photorelease of i-IP_3, whereas puffs were elicited shortly after a photolysis flash and subsequently continued to occur for tens of seconds (Fig. 1A) (*9*). The latency after which puffs are first observed shortens with increasing photorelease of IP_3 (*26*) and decreased to as little as 100 or 200 ms after strong stimuli (Fig. 1A). Figure 1B illustrates the distribution of Ca^{2+} release sites in a representative cell, in which activity was detected at a total of 18 sites after modest photorelease of i-IP_3. Ca^{2+} signals varied greatly between sites, with several locations showing frequent, large-amplitude puffs (for instance, sites 3, 8, 9, and 16), whereas others (for instance, sites 14 and 17) displayed only small, "rectangular" fluorescence blips that likely reflect openings of a single IP_3R channel (*24*). When examined on an expanded time scale, fluorescence traces showed distinct stepwise transitions during the falling phase of puffs, with dwell-state levels at approximate multiples of the unitary fluorescence level during blips (Fig. 2A). We have interpreted this quantal distribution of step amplitudes as arising from the differing numbers of IP_3R channels open at different times (*24*). Thus, it is possible to estimate the number of channels simultaneously open at the peak of a puff either by directly counting the numbers of discrete downward steps on the falling phase or by taking the ratio of the peak fluorescence amplitude divided by the unitary channel amplitude ($\Delta F/F_0$ = 0.1 ± 0.01, n = 8 sites) corresponding to blip events.

Puff amplitudes do not increase with time after photorelease of IP_3

We argue that the amplitudes of sequential puffs evoked at a given site should increase progressively with time after a photolysis flash if individual IP_3Rs are initially distributed at random but subsequently aggregate into clusters over several seconds in response to the step increase in [i-IP_3]. Figure 2B plots the peak fluorescence amplitudes of puffs as a function of time from the beginning of the UV flash: Measurements of the first puff observed at each site are indicated by filled symbols and subsequent puffs by open symbols. These data were obtained with a relatively strong flash that evoked initial puffs with short latency

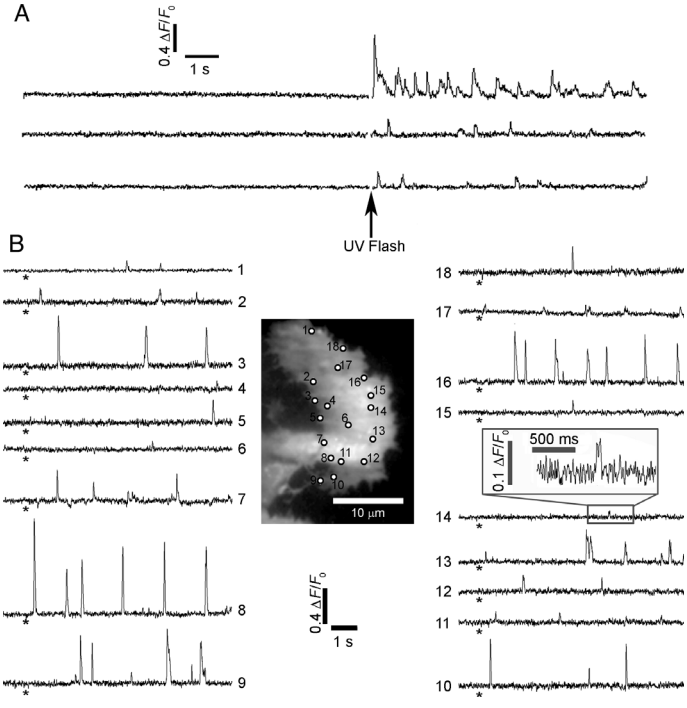

Fig. 1. Local Ca^{2+} signals evoked in SH-SY5Y cells after photorelease of i-IP_3. (**A**) Representative fluorescence traces recorded from three puff sites monitored by TIRF microscopy. Records include long baseline sections before a strong (40 ms) photolysis flash (arrow), showing a lack of basal spontaneous activity. Traces show fluorescence ratio changes ($\Delta F/F_0$) of fluo-4, monitored from 3 × 3 pixel (1 × 1 μm) regions of interest. (**B**) TIRF image shows resting fluorescence of a single fluo-4-loaded SH-SY5Y cell. Circles mark all sites at which Ca^{2+} signals were evident after photorelease of i-IP_3. Traces show fluorescence ratio signals ($\Delta F/F_0$) measured from each of the numbered sites marked on the cell image. Asterisks indicate the time of a weak (35 ms) photolysis flash. The inset box shows a single blip at site #14 with enlarged scales.

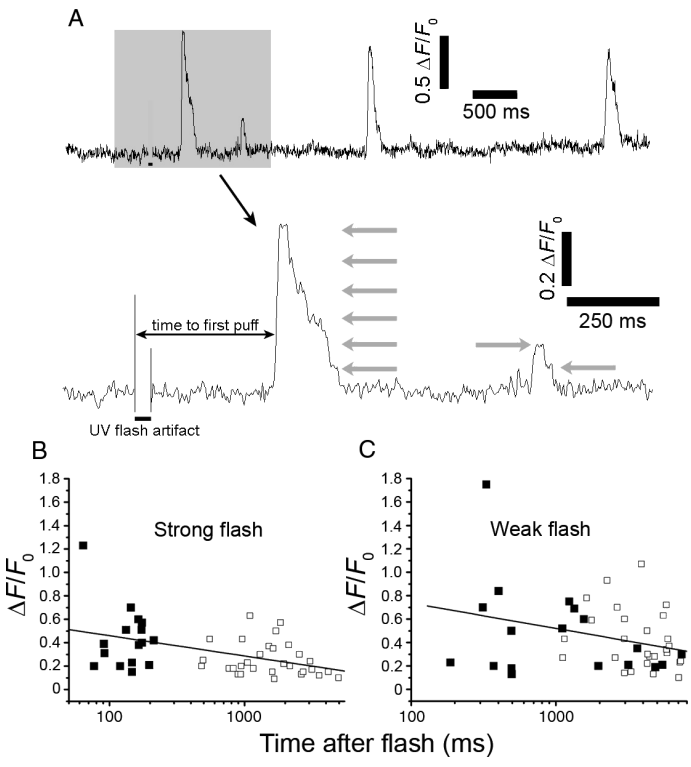

Fig. 2. Puffs evoked at short latencies after photorelease of i-IP_3 involve similar or greater numbers of IP_3R channels than do puffs observed at longer latencies. (**A**) Representative fluorescence trace ($\Delta F/F_0$) depicting the first four events evoked at a single site after a UV flash. Lower trace shows the first two events (highlighted in gray) shown on an expanded time scale showing stepwise transitions in Ca^{2+} fluorescence at approximate multiples of the unitary event level (gray arrows). Solid bars underneath each trace indicate the duration of the UV flashes. (**B** and **C**) Plots show peak puff amplitudes as a function of time after onset of the photolysis flash for strong and weak photolysis strengths, respectively. Filled squares denote the amplitude of the first event at each site, with subsequent events at those sites shown as hollow squares. Lines are regression fits to data on semilogarithmic axes.

(range, 60 to 200 ms; mean, 142 ± 10 ms; n = 16 puff sites). The mean amplitude of these short-latency puffs was $\Delta F/F_0$ = 0.44 ± 0.06, corresponding to the simultaneous opening of four to five IP_3R channels. Subsequent puffs occurring at the same sites after latencies of 0.5 to 5 s were on average somewhat smaller ($\Delta F/F_0$ = 0.26 ± 0.03, n = 30, P < 0.01; corresponding to about two to three channels), and the overall trend showed a progressive decrease in amplitude with time after the flash (Fig. 2B). Thus, it appears that on average there are already four or five IP_3Rs clustered at a puff site within 200 ms or sooner after the onset of photorelease of i-IP_3, and the observation that subsequent puffs were no larger in amplitude suggests that the number of IP_3Rs per cluster did not further increase at later times.

We wanted to determine whether the progressive decline in puff amplitude could have resulted from some mechanism that overshadowed a progressive recruitment of IP_3Rs. Degradation of photoreleased i-IP_3 is unlikely to account for the decreased puff amplitude because i-IP_3 is slowly metabolized and because puff amplitudes remain relatively undiminished over time after weak i-IP_3 photorelease (*9*). However, the large and frequent Ca^{2+} events evoked by strong photorelease of i-IP_3 tended to overpower the ability of the exogenously loaded EGTA to effectively clamp basal Ca^{2+} (*9*), resulting in a progressive increase in basal cytosolic [Ca^{2+}] (which was evident in the raw fluorescence records, but is masked by the image processing applied here) that may have inhibited IP_3Rs to cause the diminished puff amplitude. We therefore repeated these experiments using a weaker UV flash (Fig. 2C), so that basal [Ca^{2+}] remained stable. As expected (*26*), the latencies to the first puff at each site became appreciably longer (range, 200 to 4000 ms; mean, 1.9 ± 0.5 s; n = 18). Nevertheless, concordant with results obtained when the strong flash was used, puff amplitudes at shorter latencies were slightly greater than those at longer times (mean $\Delta F/F_0$ = 0.48 ± 0.09, n = 18 for puffs with latencies of 200 to 800 ms versus $\Delta F/F_0$ = 0.42 ± 0.05, n = 27 for puffs with latencies of 1 to 5 s). Moreover, we did not observe any preponderance of single-channel blip events preceding the onset of puffs, as might be expected if individual IP_3Rs were diffusing and aggregating into clusters during this time.

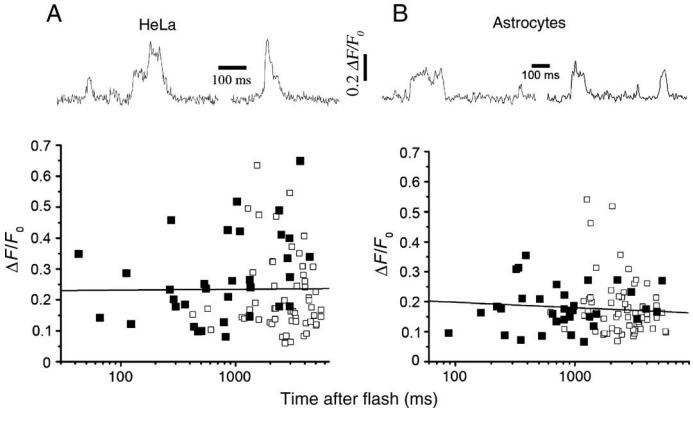

Fig. 3. Ca^{2+} signals evoked by photorelease of i-IP_3 in HeLa (**A**) and rat type I cortical astrocytes (**B**) recorded with single-channel resolution. The traces at the top show representative events displaying stepwise transitions in Ca^{2+} fluorescence. Signals in both of these cell types were on average smaller than in SH-SY5Y cells, and fewer step levels were evident. Plots show peak amplitudes of first (filled squares) and subsequent (open squares) events as functions of time after a strong (40 ms) photolysis flash. Lines are regressions to data on semilogarithmic axes.

Our measurements with TIRF microscopy provided optimal resolution of puffs, but were necessarily restricted to puff sites located adjacent to the plasma membrane that lie within the evanescent field of the microscope. To determine whether these superficial IP_3Rs might behave differently from IP_3Rs located deeper in the cell, we imaged SH-SY5Y cells by wide-field epifluorescence microscopy, focused in the center of the cells 4 to 5 μm inward from the cover glass. After evoking puffs by a photolysis flash and recording for several seconds, we rapidly switched to TIRF illumination to identify the locations of superficial puff sites so they could be excluded from analysis. Initial puffs at "deep sites" also arose after short latencies (258 ± 45 ms, n = 20 puff sites). Mean puff amplitudes showed no increase between initial and subsequent puffs at the same sites (respective amplitudes for first, second, and third puffs; $\Delta F/F_0$ = 0.61 ± 11, 0.52 ± 12, and 0.49 ± 12). Thus, the behavior of superficial puff sites imaged by TIRF microscopy in this instance appears representative of sites throughout the cell.

Puffs in HeLa cells and astrocytes imaged by TIRF microscopy

SH-SY5Y neuroblastoma cells express predominantly type I IP_3Rs (*11*, *27*), but may also contain relatively low amounts of both the type 2 (*11*, *28*) and the type 3 IP_3R (*11*, *29*). To determine whether cell lines with different proportions of IP_3R subtypes might undergo dynamic clustering, we performed similar imaging studies in HeLa cells, which are reported to contain a mixture of type 1 and type 3 IP_3Rs (*30*), and in rat astrocytes, which contain mainly type 2 IP_3Rs (*31*, *32*). TIRF imaging in both these mammalian cell types revealed stepwise changes in fluorescence reminiscent of puffs in SH-SY5Y cells (upper panels, Fig. 3, A and B). In both HeLa cells and astrocytes, mean puff amplitudes were smaller than those in SH-SY5Y cells ($\Delta F/F_0$ = 0.38 ± 0.03, n = 91 puffs in SH-SY5Y cells; 0.24 ± 0.01, n = 89, in HeLa cells; 0.18 ± 0.01, n = 91, in astrocytes). This reduced amplitude is attributable to the opening of fewer IP_3R channels, because the unitary blip amplitudes were similar among all three cell types ($\Delta F/F_0$ = 0.1 ± 0.01, n = 8; 0.1 ± 0.01, n = 15; and 0.11 ± 0.01, n = 8 for SH-SY5Y, HeLa and astrocyte cells, respectively). Nevertheless, puffs occurring within latencies of less than a few hundred milliseconds involved openings of multiple IP_3R channels, and puff amplitudes showed no appreciable increase as a function of time after photorelease of i-IP_3 in either HeLa cells or astrocytes (lower panels, Fig. 3, A and B).

Lack of motility of single IP_3Rs

To further test the hypothesis that individual IP_3Rs diffuse and aggregate into clusters after IP_3 stimulation, we examined the behavior of sites that showed repetitive single-channel activity (blips) after photorelease of i-IP_3 (Fig. 4A). We located the position of IP_3R channels with high precision by fitting a two-dimensional Gaussian function to fluorescence images of blips for every frame during which the channel was open and then calculated the mean location over successive frames during individual openings. The image in Fig. 4B shows an SH-SY5Y cell with circles marking all sites at which puffs (multi-channel Ca^{2+} signals) were observed, and the small rectangle marks the region around a blip site from which the fluorescence trace in Fig. 4A was obtained. This region is shown on an enlarged scale on the right, plotting the mean and standard error of centroid locations (centers of two-dimensional Gaussian fits) of the fluorescence signals during each of the channel openings evident in the fluorescence trace. The position of the channel deviated by no more than 300 nm during 10 s after the flash—a negligible movement compared to the ~5-μm distance to the nearest neighboring puff sites. The channel illustrated in Fig. 4A showed unusually long openings, possibly

reflecting modal gating behavior of the IP_3R (*33*), which enhanced the precision of localization. However, a similarly restricted motility was observed for other sites that displayed only brief blips (for example, site 17 in Fig. 1B). Analysis of 15 blip sites indicated an upper boundary of about 0.012 $\mu m^2\ s^{-1}$ for the two-dimensional diffusion coefficient of single IP_3Rs.

The lack of influence of IP_3 on the distribution of single IP_3Rs was further supported by an analysis of blip frequency after photo-release of i-IP_3. If IP_3 causes IP_3Rs to cluster together, we would predict that sites displaying exclusively single-channel activity would become less frequent with increasing time after photorelease of i-IP_3. This was not the case. Figure 4C plots the total numbers of blips observed within successive 2-s time bins after the photolysis flash (n = 15 blip sites in 14 cells), showing that the occurrence of blips did not diminish over the 16 s after photo-release of i-IP_3.

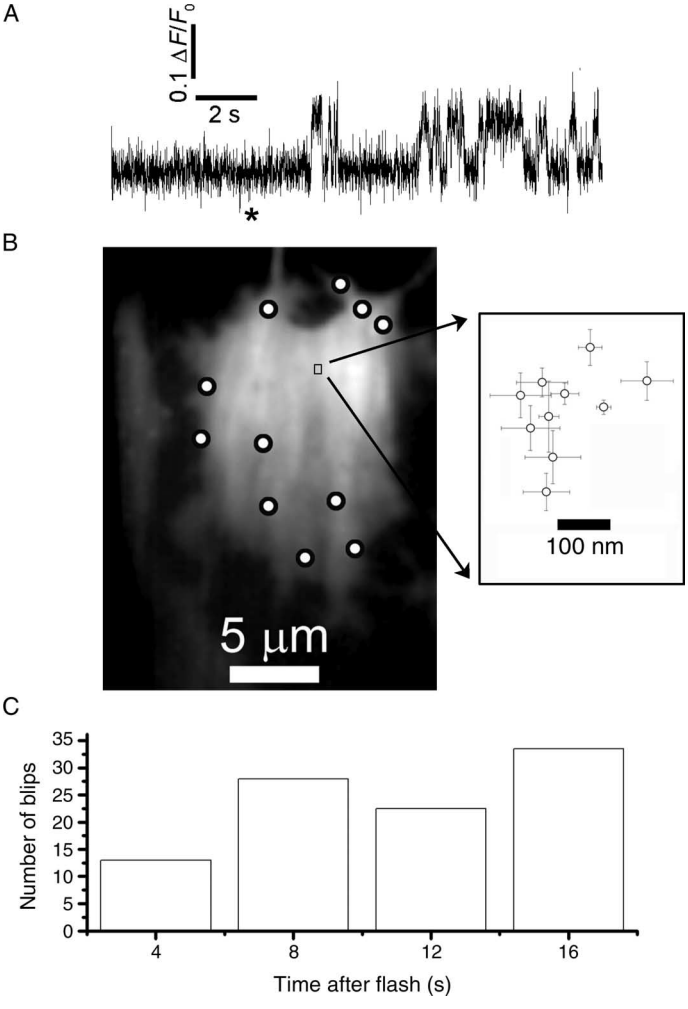

Fig. 4. Lack of motility of single IP_3Rs. (**A**) Representative trace showing activity from an apparent "lone" IP_3R after a (200 ms) photolysis flash (asterisk). Fluorescence was measured from a 1-μm^2 region of interest. (**B**) Resting fluorescence of a single fluo-4–loaded SH-SY5Y cell, with the locations of all sites showing puffs (multichannel signals) marked by circles, and with the site from which the trace in (A) was obtained marked by the box. The inset shows a scatter plot of mean centroid positions (error bars represent ± 1SEM) of Ca^{2+} fluorescence during each of the discrete openings (blips) in the trace in (A). (**C**) Bar graph shows the numbers of blips occurring during successive 2-s intervals after photorelease of i-IP_3, derived from 15 sites that displayed exclusively single-channel activity.

Modeling the diffusive aggregation of IP_3Rs

Is it possible that IP_3Rs could diffuse and aggregate into clusters within a mean time as short as 150 ms after photorelease of i-IP_3? To address this question, we performed Monte Carlo simulations of diffusive movement of IP_3Rs across the surface of the cell illustrated in Fig. 1B. We approximated the outline of the cell as a rectangle with dimensions of 10 × 20 μm and initially distributed some number N of IP_3Rs at random throughout this area. IP_3Rs were represented as circles of 20 nm diameter that diffused with a two-dimensional diffusion coefficient D. Given that puffs recur at fixed locations, we modeled cluster formation as the aggregation of IP_3Rs at defined "anchor points" corresponding to the locations of seven puff sites in the cell at which multichannel events were observed, instead of assuming that clusters arise from random association of IP_3Rs (*22*). Each anchor point represented a fixed cytoskeletal structure with diameter L. Beginning from time t = 0, we assumed that [IP_3] was instantaneously increased so that random collision of an IP_3R with an anchor point resulted in irreversible binding, and recorded the increasing numbers of IP_3Rs bound at each puff site as a function of time.

Figure 5A shows a simulation in which N was set to 100, based on an estimate of the total number of functional IP_3R in the cell of Fig. 1B obtained by counting the numbers of simultaneously open channels during the largest puff at each site plus the number of channels at "lone" sites (defined here as sites for which Ca^{2+} release from only a single IP_3R was apparent). Studies using fluorescence recovery after photobleaching (FRAP) suggest that most IP_3Rs are mobile; however, published estimates of the diffusion coefficient vary from ~0.01 to 0.45 $\mu m^2\ s^{-1}$ (*12–16*). Our own estimate (0.012 $\mu m^2\ s^{-1}$), derived from tracking functional blip sites, falls at the lower end of this range. Initially, we took a middle value of D = 0.1 $\mu m^2\ s^{-1}$, as assumed by Rahman *et al.* (*22*), and assumed a diameter of L = 20 nm for the puff anchor sites. Our experimental data (Fig. 2B) indicate that, after strong photorelease of i-IP_3, the first puffs at a given site on average involve simultaneous openings of four to five IP_3R channels, and arise after a mean latency of about 150 ms. In contrast, the simulation in Fig. 5A with the above parameter values predicts that about 1 min would pass before puff sites had, on average, accumulated four IP_3Rs.

Figure 5, B to D, shows similar simulations in which we changed one parameter value at a time, as indicated. In the simulation shown in Fig. 5B the diameter of the anchor site was increased to 300 nm, which has been estimated as the cluster size over which IP_3Rs are distributed at puff sites in oocytes (*34*). This change resulted in a modest acceleration of clustering rate; nevertheless, it took more than 30 s for an average of four IP_3Rs to accumulate in a cluster. In the simulation shown in Fig. 5C, we increased the number N of IP_3Rs per cell from 100 to 1000, while keeping D = 0.1 $\mu m^2\ s^{-1}$ and L = 20 nm. As expected, the rate of clustering was greatly accelerated, such that anchor sites had accumulated an average of about four IP_3Rs after about 4 s; however, even in this case, most anchor sites had not yet acquired even a single IP_3R after 200 ms (inset, Fig. 5C). Finally, we note that most published values of the diffusion coefficient for IP_3Rs are lower than 0.1 $\mu m^2\ s^{-1}$ (*12–14*, *16*), as is our estimate (<0.012 $\mu m^2\ s^{-1}$), based on the observed motility of blip sites. In Fig. 5D, we thus illustrate a simulation with D = 0.03 $\mu m^2\ s^{-1}$, which

predicts that it would take more than a minute before puff sites contained an average of even two IP_3Rs.

DISCUSSION

IP_3Rs are located within the membrane of the ER, which forms a contiguous network extending throughout the cytoplasm. A number of studies have indicated that a large fraction of IP_3Rs is mobile within the ER membrane (*12–20*), and that IP_3Rs are distributed uniformly at rest so that the pattern of GFP-tagged or immunostained IP_3Rs resembles that of the ER itself (*11–14*, *16–21*). It is thus surprising that functional imaging studies show that local Ca^{2+} puffs that arise from clusters of IP_3Rs remain at fixed locations over many minutes (*8–10*). Although the observation (*12*, *17–20*) that IP_3 itself induces the reversible aggregation of IP_3Rs into clusters could provide a resolution to this paradox, that explanation had never appealed to us because IP_3-induced IP_3R clustering has been described as occurring over several minutes (*12*, *17–20*), whereas puff sites are evident within a few seconds after photorelease of IP_3 (*24*, *35*). We were prompted to further examine the kinetics of establishment and stability of puff sites by a recent study (*22*) indicating that IP_3Rs in the nuclear membrane aggregate in response to increased $[IP_3]$ in as short a time as 2 s, and undergo a resulting change in channel-gating properties. On the basis of these results, the authors proposed that dynamic regulation of clustering by IP_3 facilitates hierarchical recruitment of the elementary events that underlie all IP_3-evoked Ca^{2+} signals (*22*, *23*).

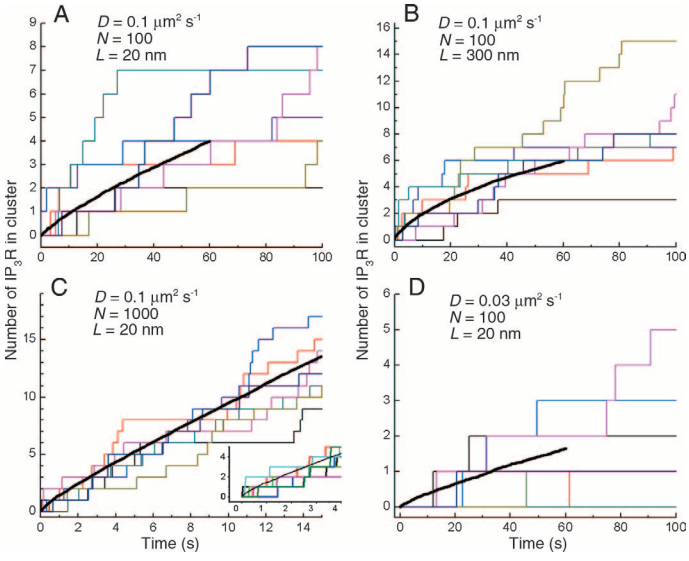

Fig. 5. Modeling cluster formation by a diffusive trap mechanism. Graphs show the numbers of IP_3Rs clustered at each of seven puff sites in a simulated cell (colored stepwise lines, with each color representing a different puff site) and the mean number of IP_3Rs per cluster (black curves; average of 50 simulations, 350 puff sites) as functions of time. The simulations model diffusion within a two-dimensional rectangular cell (10 × 20 μm) in which *N* IP_3Rs are initially distributed at random and subsequently diffuse with diffusion coefficient *D*. Seven "anchoring" sites with diameter *L* represent sites to which IP_3Rs adhere after colliding. Panels show simulations with the following respective values of *D* ($\mu m^2\ s^{-1}$), *N*, and *L* (nm): (**A**) 0.1, 100, 20; (**B**) 0,1, 100, 300; (**C**) 0.1, 1000, 20; (**D**) 0.03, 100, 20.

Here, we used a TIRF imaging technique capable of resolving the contributions of individual IP_3R channels to show that puffs involving several closely adjacent channels can be evoked within 100 to 200 ms of IP_3 stimulation in mammalian cell types with differing profiles of IP_3R subtypes. In contrast, our simulations (Fig. 5) indicate that, on the basis of reasonable assumptions for their density and diffusion coefficient, it would take many seconds or minutes for sufficient IP_3R channels to diffuse and aggregate into clusters. We thus consider it improbable that the large-amplitude, multichannel puffs we observed within a few hundred milliseconds of photorelease of IP_3 arise because IP_3Rs undergoing random walk motility redistribute under the influence of IP_3 into clusters by a diffusional trap mechanism. Moreover, our data showed various other features inconsistent with dynamic IP_3-dependent regulation of puff sites. IP_3-induced clustering is reported to result in reduction of channel mean open probability (*22*), so that a flurry of single-channel activity would be expected before IP_3Rs had time to associate into clusters. We did not observe this, even after weak photorelease of IP_3 where the clustering time may be slowed. Also, we showed that successive puffs at a given site do not grow in amplitude, as predicted for progressive recruitment of IP_3Rs, and that apparently "lone" functional IP_3Rs displayed limited motility. Together, our observations fail to support a physiological role for IP_3 in dynamically regulating IP_3R localization at puff sites in intact cells.

Is it possible, however, that clustering is still induced by IP_3, but that resting concentrations of IP_3 in the cell are already high enough to cause constitutive aggregation of IP_3R into clusters preformed before the photolysis flash? We consider this unlikely, because Ca^{2+} activity was almost nonexistent before photorelease of i-IP_3. Although we cannot exclude that some basal concentration of IP_3 is present, it would be surprising if this were sufficient to regulate IP_3R clustering and yet fail to induce any appreciable Ca^{2+} liberation. Moreover, if a low basal $[IP_3]$ were sufficient to elicit constitutive clustering of IP_3Rs, this would leave little role for stimulus-induced IP_3R clustering.

How then might our data be reconciled with several studies suggesting that a substantial population of IP_3Rs is freely diffusible within the ER membrane (*12–20*) and undergo a global reorganization after stimulation? (*12*, *17–20*, *36*). One possibility is that our stimuli did not increase cytosolic $[IP_3]$ sufficiently to effect IP_3R clustering. However, this seems unlikely because, although cells were loaded with the slow Ca^{2+} buffer EGTA to deliberately inhibit cluster-cluster interactions and suppress global Ca^{2+} waves, photolysis flash strengths equivalent to or weaker than those used here produce robust and long-lasting (minutes) global increases in cytosolic free $[Ca^{2+}]$ in the absence of EGTA (*9*).

We believe that a more likely explanation is that we monitored those IP_3Rs that show functional Ca^{2+} release under minimally invasive conditions, whereas most previous studies localized IP_3R proteins either by tagging exogenously expressed receptors with fluorescent proteins, by immunostaining endogenous IP_3Rs, or by both of these methods (*11–20*). As noted above, both of these approaches show IP_3Rs distributed widely throughout the ER [see, for example, (*12*, *18*, *20*)]. On this basis, one would expect that IP_3-evoked Ca^{2+} release would be apparent throughout the cell cytoplasm; however, numerous studies have indicated that this is not the case. Instead, Ca^{2+} release in various cells arises at just a few discrete puff sites (*9–11*, *24*, *37*, *38*), which appear to be anchored in place because they do not move even in the face of sustained increases in $[IP_3]$ that evoke repetitive Ca^{2+} waves (*39*). We thus propose that cells may contain two different populations of IP_3Rs: (i) a subset of receptors that are anchored together in preformed clusters by association with static cytoskeletal structures and which, possibly as a consequence of this anchoring, display high sensitivity to IP_3 to generate Ca^{2+} puffs; (ii) a population of mobile IP_3Rs that are either functionally unresponsive,

or mediate Ca^{2+} liberation only during sustained global increases of cytosolic [Ca^{2+}]. Our proposed scheme involves modulation of IP_3R function based on their localization, but in the opposite sense to that proposed by Rahman *et al*. (*22*). That is, in our scheme, clustered IP_3R are preferentially activated under conditions that evoke puffs, rather than displaying a reduced open-channel probability.

Cellular Ca^{2+} signaling is a highly regulated process, with localized increases in [Ca^{2+}] playing widely divergent physiological and pathophysiological roles depending on where in the cytosol these localized signals arise (*1*). We provide evidence indicating that the sites generating local Ca^{2+} puffs represent preestablished, stable clusters of IP_3Rs; and further speculate that puff sites may be defined by the functional modulation and immobilization of IP_3Rs from a larger pool of diffusionally mobile receptors when they bind to static cytoskeletal elements.

METHODS

Cell culture

Human SH-SY5Y neuroblastoma cells were cultured as previously described (*9*) in a mixture (1:1) of Ham's F12 medium and Eagle's minimal essential medium supplemented with 10% (v/v) fetal bovine serum (FBS) and 1% nonessential amino acids. Cells were incubated at 37°C in a humidified incubator with a 95% air and 5% CO_2 atmosphere, passaged every 7 days, and used for up to 20 passages. A few days before imaging, cells were harvested in phosphate-buffered saline (PBS) without Ca^{2+} or Mg^{2+} and subcultured in petri dishes with glass coverslips as the base (MatTek) at a seeding density of 3×10^4 cells/ml. HeLa cells were cultured in a similar manner except that the culture medium consisted of Dulbecco's modified Eagle's medium (DMEM) supplemented with 10% FBS and 1% penicillin-streptomycin.

To obtain astrocytes, cerebral cortices were removed from four 1- to 3-day-old Sprague-Dawley rat pups and placed immediately in ice-cold buffer solution consisting of 10 mM NaH_2PO_4, 2.7 mM KCl, 137 mM NaCl, 14 mM glucose, 1.5 mM $MgSO_4$, and bovine serum albumin (3 mg/ml). Meninges were removed with fine forceps; whole cortices were then minced using fine forceps and placed into 0.125% trypsin-EDTA for 10 min. Trypsin digestion was halted by the addition of an equal volume of fresh astrocyte culture media (DMEM supplemented with 10% FBS and 1% penicillin-streptomycin). The tissue was then pelleted by centrifugation at 4500 rpm for 5 min, after which the supernatant was removed and the cell pellet resuspended in 2 ml of fresh medium. The tissue was subsequently triturated gently with three fire-polished Pasteur pipettes of narrowing bore size. Larger pieces of tissue were allowed to settle for 5 min, after which the supernatant was applied to a 40-μm cell strainer and 40 ml of fresh medium was applied. This cell suspension was then aliquoted into 1×25-cm^2 flasks and onto petri dishes with glass coverslips as the base (MatTek). Cells were then kept in a humidified incubator at 37°C (95% air, 5% CO_2). This was designated passage 1, and cells were used up to a passage of 2. Four to six hours after plating, cells were washed vigorously several times with fresh medium to remove nonadhered cells. This resulted in a culture of primarily type I cortical astrocytes [as confirmed by positive immunostaining with antibody directed against glial fibrillary acidic protein (GFAP)]. Culture medium was exchanged every 3 to 4 days and cells were grown in culture for up to 14 days. All recordings were made from cells between days 5 to 12.

Loading of cell-permeant esters

Cells were loaded a few hours before use by incubation with Hepes-buffered saline [HBS (in mM): NaCl 135, KCl 5, $MgCl_2$ 1.2, $CaCl_2$ 2.5, Hepes 5, glucose 10] containing 1 μM ci-IP_3-(propionyloxymethyl)ester (ci-IP_3/PM) (SiChem) at room temperature for 45 min, followed by incubation with 1 μM caged ci-IP_3/PM plus 5 μM fluo-4AM (Invitrogen) at room temperature for 45 min, and, finally, for 1 hour with 5 μM EGTA acetoxymethyl ester (Invitrogen).

Total internal reflection microscopy

Imaging of changes in intracellular calcium concentration ([Ca^{2+}]$_i$) was accomplished with a custom-built TIRF microscope system based around an Olympus IX 70 microscope equipped with an Olympus X60 TIRFM objective [NA (numerical aperture) 1.45). Fluorescence of cytosolic fluo-4 was excited within the ~100-nm evanescent field formed by total internal reflection of a 488-nm laser beam incident through the microscope objective at the coverglass-aqueous interface. Images of emitted fluorescence (λ >510 nm) were captured at a resolution of 128 × 128 pixels (1 pixel = 0.4 μm) at a rate of 420 frames per second by a Cascade 128 electron multiplied CCD (charge-coupled device) camera (Roper Scientific). Photorelease of i-IP_3 from a caged precursor was evoked by flashes of UV (350–400 nm) light derived from a fiber-optic arc lamp source introduced through a UV-reflecting dichroic mirror in the upper side port of the microscope. The UV light was adjusted to uniformly irradiate a region slightly larger than the imaging frame, and any given imaging field was exposed to only a single flash.

Image processing and analysis

Image processing and analysis were done with MetaMorph 7.5 (Molecular Dynamics). After subtraction of the camera black offset level, image sequences were first processed by dividing each frame by an average of ~100 frames captured before the photolysis flash, so that fluorescence represents a ratio ($\Delta F/F_0$) of the fluorescence change (ΔF) at each pixel relative to the mean resting fluorescence (F_0) before stimulation. The resulting image stack was then further processed by frame-by-frame subtraction of heavily smoothed (16 × 16 pixel low-pass filter) images to correct for slow drift in basal fluorescence and fluctuations in laser power (*40*). Fluorescence traces like those in Fig. 1 were derived by measuring the average signal within 1.2 × 1.2 μm (3 × 3 pixel) regions of interest centered on visually identified Ca^{2+} release sites. Puff latencies are expressed as the time from onset of the photolysis flash to onset of the puff. Single-channel Ca^{2+} fluorescence signals were localized by fitting to a circularly symmetrical Gaussian function with a precision of 0.2 pixels, using a custom particle-tracking routine in Slidebook (Intelligent Imaging Innovations). The amplitude was allowed to vary to achieve the best fit whereas the standard deviation was preset to 3 pixels (1.2 μm). Diffusion coefficients D were calculated from a regression fit to data plotting displacements of puff centroids as a function of time as $D = d2/4t$, where d = mean distance of the blip fluorescence during each opening from its origin at time t.

Stochastic simulation of IP_3R diffusion and clustering

The ER membrane within the plane of the TIRF image was simulated as a two-dimensional rectangular domain with a size of 10 × 20 μm. A certain number N of IP_3R channels with diameter 20 nm were randomly distributed on the ER membrane at time $t = 0$ and underwent a random walk in both x and y directions by incrementing their positions at time steps Δt = 10 μs by adding random numbers distributed as a Gaussian function centered around zero. The width (standard deviation) of the Gaussian was adjusted to achieve the desired macroscopic diffusion coefficients. IP_3Rs hitting the boundaries were reflected back. For simplicity, we ignored collisions among IP_3Rs; that is, IP_3Rs passed through each other without deflection. Specific fixed anchor sites were designated as IP_3R channel trap locations, based on the mapping in Fig. 1B. Each trap location was

assumed to have a diameter L. An IP_3R channel moving within a distance of $L/2 + 10$ nm became fixed at that anchor site. For simplicity, we assumed that trapped channels did not affect the trap diameter or location. Figure 5 shows the results of representative single simulations, counting the numbers of IP_3Rs trapped at each site as a function of time t, together with mean numbers of IP_3R per cluster derived from 50 simulations.

REFERENCES AND NOTES

1. M. J. Berridge, P. Lipp, M. D. Bootman, The versatility and universality of calcium signalling. *Nat. Rev. Mol. Cell Biol.* **1**, 11–21 (2000).
2. J. K. Foskett, C. White, K. H. Cheung, D. O. Mak, Inositol trisphosphate receptor Ca^{2+} release channels. *Physiol. Rev.* **87**, 593–658 (2007).
3. I. Bezprozvanny, J. Watras, B. E. Ehrlich, Bell-shaped calcium-response curves of Ins(l,4,5)P_3- and calcium-gated channels from endoplasmic reticulum of cerebellum. *Nature* **351**, 751–754 (1991).
4. P. Lipp, E. Niggli, A hierarchical concept of cellular and subcellular Ca^{2+}-signalling. *Prog. Biophys. Mol. Biol.* **65**, 265–296 (1996).
5. I. Parker, J. Choi, Y. Yao, Elementary events of $InsP_3$-induced Ca^{2+} liberation in *Xenopus* oocytes: Hot spots, puffs and blips. *Cell Calcium* **20**, 105–121 (1996).
6. Y. Yao, J. Choi, I. Parker, Quantal puffs of intracellular Ca^{2+} evoked by inositol trisphosphate in *Xenopus* oocytes. *J. Physiol.* **482**, 533–553 (1995).
7. J. W. Shuai, P. Jung, Optimal ion channel clustering for intracellular calcium signaling. *Proc. Natl. Acad. Sci. U.S.A.* **100**, 506–510 (2003).
8. S. L. Dargan, I. Parker, Buffer kinetics shape the spatiotemporal patterns of IP_3-evoked Ca^{2+} signals. *J. Physiol.* **553**, 775–788 (2003).
9. I. F. Smith, S. M. Wiltgen, I. Parker, Localization of puff sites adjacent to the plasma membrane: Functional and spatial characterization of Ca^{2+} signaling in SH-SY5Y cells utilizing membrane-permeant caged IP_3. *Cell Calcium* **45**, 65–76 (2009).
10. D. Thomas, P. Lipp, M. J. Berridge, M. D. Bootman, Hormone-evoked elementary Ca^{2+} signals are not stereotypic, but reflect activation of different size channel clusters and variable recruitment of channels within a cluster. *J. Biol. Chem.* **273**, 27130–27136 (1998).
11. S. C. Tovey, P. de Smet, P. Lipp, D. Thomas, K. W. Young, L. Missiaen, H. De Smedt, J. B. Parys, M. J. Berridge, J. Thuring, A. Holmes, M. D. Bootman, Calcium puffs are generic $InsP_3$-activated elementary calcium signals and are downregulated by prolonged hormonal stimulation to inhibit cellular calcium responses. *J. Cell Sci.* **114**, 3979–3989 (2001).
12. M. Chalmers, M. J. Schell, P. Thorn, Agonist-evoked inositol trisphosphate receptor (IP_3R) clustering is not dependent on changes in the structure of the endoplasmic reticulum. *Biochem. J.* **394**, 57–66 (2006).
13. C. Cruttwell, J. Bernard, M. Hilly, V. Nicolas, R. E. Tunwell, J. P. Mauger, Dynamics of the Ins(1,4,5)P_3 receptor during polarization of MDCK cells. *Biol. Cell* **97**, 699–707 (2005).
14. M. Ferreri-Jacobia, D. O. Mak, J. K. Foskett, Translational mobility of the type 3 inositol 1,4,5-trisphosphate receptor Ca^{2+} release channel in endoplasmic reticulum membrane. *J. Biol. Chem.* **280**, 3824–3831 (2005).
15. K. Fukatsu, H. Bannai, S. Zhang, H. Nakamura, T. Inoue, K. Mikoshiba, Lateral diffusion of inositol 1,4,5-trisphosphate receptor type 1 is regulated by actin filaments and 4.1N in neuronal dendrites. *J. Biol. Chem.* **279**, 48976–48982 (2004).
16. C. J. Gibson, B. E. Ehrlich, Inositol 1,4,5-trisphosphate receptor movement is restricted by addition of elevated levels of O-linked sugar. *Cell Calcium* **43**, 228–235 (2008).
17. M. Iwai, Y. Tateishi, M. Hattori, A. Mizutani, T. Nakamura, A. Futatsugi, T. Inoue, T. Furuichi, T. Michikawa, K. Mikoshiba, Molecular cloning of mouse type 2 and type 3 inositol 1,4,5-trisphosphate receptors and identification of a novel type 2 receptor splice variant. *J. Biol. Chem.* **280**, 10305–10317 (2005).
18. Y. Tateishi, M. Hattori, T. Nakayama, M. Iwai, H. Bannai, T. Nakamura, T. Michikawa, T. Inoue, K. Mikoshiba, Cluster formation of inositol 1,4,5-trisphosphate receptor requires its transition to open state. *J. Biol. Chem.* **280**, 6816–6822 (2005).
19. Y. Tojyo, T. Morita, A. Nezu, A. Tanimura, The clustering of inositol 1,4,5-trisphosphate (IP_3) receptors is triggered by IP_3 binding and facilitated by depletion of the Ca^{2+} store. *J. Pharmacol. Sci.* **107**, 138–150 (2008).
20. B. S. Wilson, J. R. Pfeiffer, A. J. Smith, J. M. Oliver, J. A. Oberdorf, R. J. Wojcikiewicz, Calcium-dependent clustering of inositol 1,4,5-trisphosphate receptors. *Mol. Biol. Cell* **9**, 1465–1478 (1998).
21. S. Kume, A. Muto, J. Aruga, T. Nakagawa, T. Michikawa, T. Furuichi, S. Nakade, H. Okano, K. Mikoshiba, The *Xenopus* IP_3 receptor: Structure, function, and localization in oocytes and eggs. *Cell* **73**, 555–570 (1993).
22. Taufiq-Ur-Rahman, A. Skupin, M. Falcke, C. W. Taylor, Clustering of $InsP_3$ receptors by $InsP_3$ retunes their regulation by $InsP_3$ and Ca^{2+}. *Nature* **458**, 655–659 (2009).
23. T. Rahman, C. W. Taylor, Dynamic regulation of IP_3 receptor clustering and activity by IP_3. *Channels (Austin)* **3**, 226–232 (2009).
24. I. F. Smith, I. Parker, Imaging the quantal substructure of single IP_3R channel activity during Ca^{2+} puffs in intact mammalian cells. *Proc. Natl. Acad. Sci. U.S.A.* **106**, 6404–6409 (2009).
25. J. Shuai, I. Parker, Optical single-channel recording by imaging Ca^{2+} flux through individual ion channels: Theoretical considerations and limits to resolution. *Cell Calcium* **37**, 283–299 (2005).
26. N. Callamaras, J. S. Marchant, X. P. Sun, I. Parker, Activation and co-ordination of $InsP_3$-mediated elementary Ca^{2+} events during global Ca^{2+} signals in *Xenopus* oocytes. *J. Physiol.* **509**, 81–91 (1998).
27. R. J. Wojcikiewicz, Type I, II, and III inositol 1,4,5-trisphosphate receptors are unequally susceptible to down-regulation and are expressed in markedly different proportions in different cell types. *J. Biol. Chem.* **270**, 11678–11683 (1995).
28. J. J. Mackrill, R. A. Challiss, D. A. O'Connell, F. A. Lai, S. R. Nahorski, Differential expression and regulation of ryanodine receptor and *myo*-inositol 1,4,5-trisphosphate receptor Ca^{2+} release channels in mammalian tissues and cell lines. *Biochem. J.* **327**, 251–258 (1997).
29. K. Van Acker, N. Nadif Kasri, P. De Smet, J. B. Parys, H. De Smedt, L. Missiaen, G. Callewaert, IP_3-mediated Ca^{2+} signals in human neuroblastoma SH-SY5Y cells with exogenous overexpression of type 3 IP_3 receptor. *Cell Calcium* **32**, 71–81 (2002).
30. M. Hattori, A. Z. Suzuki, T. Higo, H. Miyauchi, T. Michikawa, T. Nakamura, T. Inoue, K. Mikoshiba, Distinct roles of inositol 1,4,5-trisphosphate receptor types 1 and 3 in Ca^{2+} signaling. *J. Biol. Chem.* **279**, 11967–11975 (2004).
31. L. A. Holtzclaw, S. Pandhit, D. J. Bare, G. A. Mignery, J. T. Russell, Astrocytes in adult rat brain express type 2 inositol 1,4,5-trisphosphate receptors. *Glia* **39**, 69–84 (2002).
32. J. Petravicz, T. A. Fiacco, K. D. McCarthy, Loss of IP_3 receptor-dependent Ca^{2+} increases in hippocampal astrocytes does not affect baseline CA1 pyramidal neuron synaptic activity. *J. Neurosci.* **28**, 4967–4973 (2008).
33. L. Ionescu, C. White, K. H. Cheung, J. Shuai, I. Parker, J. E. Pearson, J. K. Foskett, D. O. Mak, Mode switching is the major mechanism of ligand regulation of $InsP_3$ receptor calcium release channels. *J. Gen. Physiol.* **130**, 631–645 (2007).
34. J. Shuai, H. J. Rose, I. Parker, The number and spatial distribution of IP_3 receptors underlying calcium puffs in *Xenopus* oocytes. *Biophys. J.* **91**, 4033–4044 (2006).
35. X. P. Sun, N. Callamaras, J. S. Marchant, I. Parker, A continuum of $InsP_3$-mediated elementary Ca^{2+} signalling events in *Xenopus* oocytes. *J. Physiol.* **509**, 67–80 (1998).
36. S. L. Dargan, A. Demuro, I. Parker, Imaging Ca^{2+} signals in *Xenopus* oocytes. *Methods Mol. Biol.* **322**, 103–119 (2006).
37. M. Bootman, E. Niggli, M. Berridge, P. Lipp, Imaging the hierarchical Ca^{2+} signalling system in HeLa cells. *J. Physiol.* **499**, 307–314 (1997).
38. M. D. Bootman, M. J. Berridge, P. Lipp, Cooking with calcium: The recipes for composing global signals from elementary events. *Cell* **91**, 367–373 (1997).
39. J. S. Marchant, I. Parker, Role of elementary Ca^{2+} puffs in generating repetitive Ca^{2+} oscillations. *EMBO J.* **20**, 65–76 (2001).
40. A. Demuro, I. Parker, "Optical patch-clamping": Single-channel recording by imaging Ca^{2+} flux through individual muscle acetylcholine receptor channels. *J. Gen. Physiol.* **126**, 179–192 (2005).

41. We thank K. Kilborn (Intelligent Imaging Innovations) for writing the custom localization routine. This work was supported by grants GM 48071 and GM 65830 from the NIH and by a University of California Systemwide Biotechnology Research & Education Program GREAT Training Grant 2008-14 to S.W.

Submitted 12 June 2009
Accepted 5 November 2009
Final Publication 24 November 2009
10.1126/scisignal.2000466
Citation: I. F. Smith, S. M. Wiltgen, J. Shuai, I. Parker, Ca^{2+} puffs originate from preestablished stable clusters of inositol trisphosphate receptors. *Sci. Signal.* **2**, ra77 (2009).